LETTER TO THE EDITOR

HR 6819 is a binary system with no black hole[★]

Revisiting the source with infrared interferometry and optical integral field spectroscopy

A. J. Frost[1], J. Bodensteiner[2], Th. Rivinius[3], D. Baade[2], A. Merand[2], F. Selman[3], M. Abdul-Masih[3], G. Banyard[1], E. Bordier[1,3], K. Dsilva[1], C. Hawcroft[1], L. Mahy[4], M. Reggiani[1], T. Shenar[5], M. Cabezas[6], P. Hadrava[6], M. Heida[2], R. Klement[7] and H. Sana[1]

[1] Institute of Astronomy, KU Leuven, Celestijnlaan 200D, 3001 Leuven, Belgium
e-mail: afrost274@gmail.com
[2] European Organisation for Astronomical Research in the Southern Hemisphere (ESO), Karl-Schwarzschild-Str. 2, 85748 Garching b. München, Germany
[3] European Organisation for Astronomical Research in the Southern Hemisphere (ESO), Casilla 19001, Santiago 19, Chile
[4] Royal Observatory of Belgium, Avenue Circulaire 3, B-1180 Brussel, Belgium
[5] Anton Pannekoek Institute for Astronomy, University of Amsterdam, Postbus 94249, 1090 GE Amsterdam, The Netherlands
[6] Astronomical Institute, Academy of Sciences of the Czech Republic, Bočni II 1401, 141 31 Praha 4, Czech Republic
[7] The CHARA Array of Georgia State University, Mount Wilson Observatory, Mount Wilson, CA 91023, USA

ABSTRACT

Context. Two scenarios have been proposed to match the existing observational constraints of the object HR 6819. The system could consist of a close inner B-type giant + black hole (BH) binary with an additional Be companion on a wide orbit. Alternatively, it could be a binary composed of a stripped B star and a Be star in a close orbit. Both scenarios make HR 6819 a cornerstone object, either as the closest stellar BH to Earth, or as an example of an important transitional, non-equilibrium phase for Be stars with solid evidence to back its nature.
Aims. We aim to distinguish between the two scenarios for HR 6819. Both models predict two luminous stars but with very different angular separations and orbital motions. Therefore, the presence of bright sources in the 1-100 milli-arcsec (mas) regime is a key diagnostic to determine the nature of the HR 6819 system.
Methods. We obtained new high-angular resolution data with VLT/MUSE and VLTI/GRAVITY of HR 6819. The MUSE data are sensitive to bright companions at large scales, whilst the interferometric GRAVITY data are sensitive down to separations of order mas scales and large magnitude differences.
Results. The MUSE observations reveal no bright companion at large separations and the GRAVITY observations indicate the presence of a stellar companion at an angular separation of ~ 1.2 mas, moving on the plane of the sky over a time scale compatible with the known spectroscopic 40 day period.
Conclusions. We conclude that HR 6819 is a binary system and that no BH is present in the system. The unique nature of HR 6819, and its proximity to Earth make it an ideal system to quantitatively characterise the immediate outcome of binary interaction and probe how Be stars form.

Key words. Stars: individual: HR 6819 - Stars: massive - Stars: emission-line, Be - Binaries: close - Techniques: interferometric - Techniques: imaging spectroscopy

1. Introduction

The majority of main-sequence (MS) massive OB-type stars belong to binary or higher order multiple systems, among which close binaries ($P < 10$ yrs) are common (Mason et al. 1998; Sana et al. 2012; Sota et al. 2014; Moe & Di Stefano 2017; Almeida et al. 2017; Banyard et al. 2021; Villaseñor et al. 2021). Close companions will most likely interact and exchange mass and angular momentum, significantly impacting their subsequent evolutionary path and final fates. Binary interactions are likely to leave the involved stars chemically and physically al-

tered (Paczyński 1971; Pols et al. 1991; de Mink et al. 2013), although high quality observations to confront theoretical predictions are lacking (Mahy et al. 2020a,b). If the central core is massive enough and the system survives both the interaction and a potential supernova explosion, it may result in a MS + compact object binary (Langer et al. 2020). Those are prime candidate progenitors of high- and low-mass X-ray binaries (e.g. Liu et al. 2006) and, for a small fraction of them, of double compact binaries and gravitational wave (GW) mergers (e.g. Abbott et al. 2019).

HR 6819 (also known as HD 167 128, ALS 15 056, and QV Tel) is a highly intriguing object which was recently proposed as a candidate multiple system containing a stellar-mass black-hole (BH). Based on optical spectroscopic monitoring

---

over ~5yrs, Rivinius et al. (2020) determined HR 6819 to be a narrow, singled-lined spectroscopic binary with a 40-d orbit and a negligible eccentricity. The authors proposed the HR 6819 system to be a hierarchical triple, with a distant classical Be star orbiting a short-period inner binary consisting of a B3 III star and a stellar, quiescent (non-accreting) BH in a close circular orbit. Classical Be stars are rapidly-rotating B stars with decretion disks which produce strong emission lines (e.g. Rivinius et al. 2013), with studies suggesting that they may form as a result of mass- and angular momentum transfer in binary systems (e.g. Wang et al. 2021; Bodensteiner et al. 2020b; Klement et al. 2019). This would make HR 6819 a lower mass counterpart of LB-1, another intriguing spectroscopic binary system (Irrgang et al. 2020). While early works implied that the detected RV signal was spurious and a more conservative mass BH could reproduce the observations of LB-1 (Abdul-Masih et al. 2020; El-Badry & Quataert 2020; Simón-Díaz et al. 2020), Shenar et al. (2020) showed that the spectral variations could instead be due to a rare Be binary system consisting of a stripped star and a Be star rotating near its critical velocity. **Both models were additionally tested by Lennon et al. (2021).**

For HR 6819, Bodensteiner et al. (2020a) and El-Badry & Quataert (2021) independently proposed that the spectral observations could similarly be caused by a binary system consisting of a stripped B-type primary and a rapidly-rotating Be star that formed from a previous mass-transfer event. Additionally, Gies & Wang (2020) reported a small reflex motion detected in the Hα line arising in the Be star disk, invoked by a companion on a close orbit, therefore yielding the same conclusion. In the meantime, Safarzadeh et al. (2020) proposed, based on stability arguments, that the triple configuration is highly unlikely. On the other hand, Mazeh & Faigler (2020) argued that if HR 6819 is indeed a triple system, the putative BH could itself be an undetected binary system of two A0 stars, making HR 6819 a quadruple system. Klement et al. (2021) later reported on speckle observations (obtained with the Zorro imager on the Gemini South telescope in Chile) that indicated a possible optical source at 120 milli-arcsec (mas) from the central source. Given that the brightness of the source could not be fully constrained (it can be up to five magnitudes fainter than the central object), it could either be the Be star and thus an indication for the triple scenario, or an unrelated background or foreground source.

The main difference between the two main proposed scenarios (the triple interpretation with an inner BH+B star binary and an outer Be star - Rivinius et al. (2020), and the binary interpretation with a low-mass stripped star and a Be star in a close binary - Bodensteiner et al. 2020a; El-Badry & Quataert 2021) is the separation of the two luminous sources. The triple scenario relies on a wide orbit for the two bright stars in the system with an angular separation around ~100 mas, so that significant shifts are not generated in the RV measurements over 5 years. On the other hand, the binary model requires a much smaller separation of ~1-2 mas. Both models have consequential implications. Should HR 6819 contain a BH, the system constitutes a prime testing centre to investigate supernova kicks and GW-progenitors. Should HR 6819 contain a stripped star, this provides a direct observation of a binary system briefly after mass transfer as well as evidence for the binary channel as an avenue to forming classical Be stars.

In this letter we present new observations of HR 6819 designed to distinguish between these two scenarios. Specifically, GRAVITY/VLTI and MUSE/VLT observations were selected. The MUSE data are sensitive to a wide companion, with separations in the range of ~100 mas to 7.5", whilst the GRAVITY data cover the range from a fraction of a mas to ~100 mas. In Sections 2 and 3, we present our MUSE and GRAVITY observations respectively. Our results are discussed and summarised in Section 4, where we offer our conclusion that HR 6819 is a close binary consisting of a stripped B star and a rapidly rotating Be star.

2. MUSE: The search for a wide companion

2.1. Observational setup and data reduction

MUSE, the Multi Unit Spectroscopic Explorer at the UT4 telescope at the Very Large Telescope (VLT), is an integral field spectrograph operating over visible wavelengths (480-930nm) (Bacon et al. 2010). The MUSE observations were designed to detect a possible wide companion. The spectroscopic observations implied that the B star and Be star are of similar brightness (Rivinius et al. 2020; Bodensteiner et al. 2020a), and the speckle interferometry suggested a source at most five magnitudes fainter than the central source at a separation of 120 mas (Klement et al. 2021). Therefore, the observations were set up to yield a signal-to-noise (S/N) ratio of 25 in Hα for a putative companion at 120 mas that is five magnitudes fainter than the central source.

One epoch of VLT/MUSE observations of HR 6819 was obtained on July 22, 2021 (2107.D-5026, PI: Rivinius) in the narrow-field mode (NFM), supported by adaptive optics (AO), and in nominal wavelength mode (N). The NFM covers a 7.5" × 7.5" field-of-view (FoV) with a spatial sampling of 0.025" × 0.025". At a distance of 340 pc, the FoV corresponds to ~2550 AU (or ~0.12 pc). Given the brightness of the target (V = 5.4), the observations were not carried out in the normal NFM-AO mode but using a procedure which widens the laser configuration and thus allows the observations of brighter stars. The observation was split into several subsets with a small (~1") offset and position angle 0 or 90°. Each set was then made up by 6 or 12 short (3-second) exposures, leading to a total of 36 exposures with an overall exposure time of 108 seconds.

The individual MUSE-NFM-AO-N observations were reduced using the standard MUSE pipeline (Weilbacher et al. 2020) which includes bias subtraction, flat fielding, wavelength calibration and illumination correction for each individual integral field unit (IFU). After recombining the data subsets from all the IFUs, the data were flux-calibrated using a standard star and a sky subtraction was performed. Given the extremely good weather conditions during the observations (at the start of the first exposure, the seeing was 0.58", which varied between the observations and increased to around 0.86"), most of the exposures are saturated in the central source. This, however, does not affect the purpose of the MUSE observations, which is to probe whether there is a wide companion at ~120 mas.

2.2. Results

The individual (not-saturated) MUSE exposures show one central source. Collapsing the wavelengths to a white-light image (see Figure A.1) we find no indication for a second bright source at 120 mas. Using the spectroscopic capabilities of MUSE, we find no indication for a second star further out (which could for example be indicated by spatially localised absorption lines in the Ca triplet at around 8500 Å). Additionally, there seems to be no significant spatial change of the spectrum of the central source so we extract the spectrum by summing over the 3×3
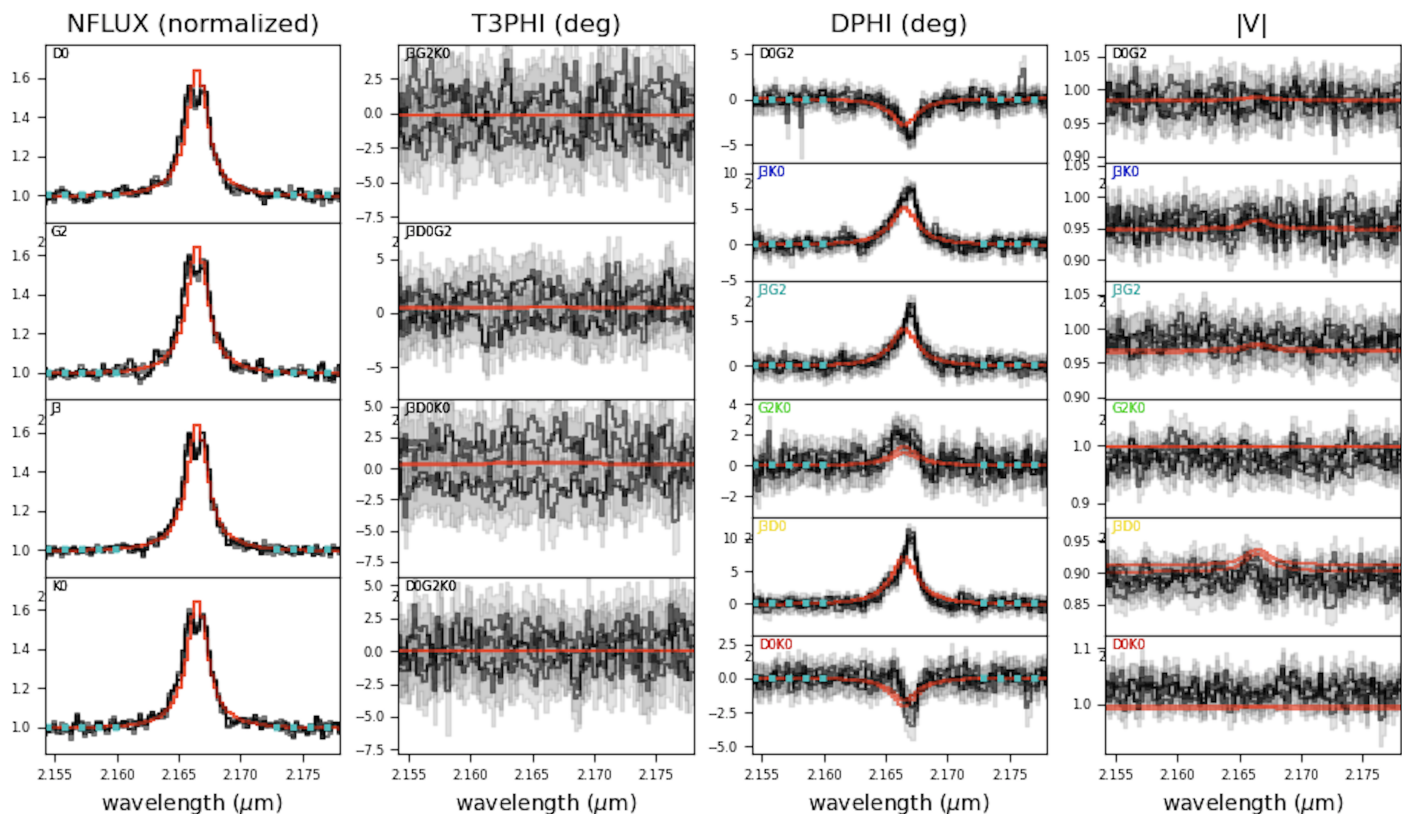
Fig. 1. Best-fits to the GRAVITY dataset taken on September 19 2021 formed from a model composed of two point sources. The data are shown in black and the model in red over a wavelength range highlighting the Brγ region as opposed to the whole GRAVITY wavelength range. In the appendices, we explain in detail how we determine this as our final fit to the data. While the different rows show different VLTI baselines (see inset labels), the different panels show the normalized flux, the closure phases, the differential phases as well as the visibilities, from left to right. The blue dots represent the continuum.

most central pixels with QFitsView[1]. We compare this extracted spectrum to an observed FEROS spectrum. (described in Rivinius et al. 2020) at a similar orbital phase, after resampling them to the MUSE resolution and binning. The comparison (**see Fig. A.2**) shows that there is no significant difference between the spectra taken by the two instruments, implying that the two sources which contribute to the composite FEROS spectrum (the B and the Be star, which are common to both models) are both located within in the central source detected in the MUSE data.

These two findings combined (i.e. the lack of a second bright source at 120 mas from the central source, and the fact that both B and Be star contribute to the spectrum of the central source) unambiguously show that the Be star in HR 6819 is not a wide companion located at 120 mas as suggested by the speckle interferometry.

3. GRAVITY: Probing the inner regions

3.1. Observations and fitting process

GRAVITY is the K-band 4-telescope beam combiner at the Very Large Telescope Interferometer (VLTI, Gravity Collaboration et al. 2017). Three GRAVITY observations of HR 6819 were obtained in August and September 2021 using the high spectral resolving power setting of GRAVITY ($R = \lambda/\Delta\lambda = 4000$). Observations were taken with the large configuration (A0-G1-J2-J3) of the 1.8 m Auxiliary Telescopes (ATs). The first observation (August 2021) was unsuccessful, as severe weather and

technical issues only allowed the science source to be observed with no calibrator. The following two attempts, on September 6th and 19th 2021, were however successful, with clear sky conditions, precipitable water vapour below 30 mm, and seeing of less than 1" for both the science source and the calibrator star (HD 161420). The data were reduced and calibrated using the standard GRAVITY pipeline (Lapeyrere et al. 2014).

Geometric fitting was applied to the interferometric observables (i.e., visibilities, closure phases, differential phases and normalised fluxes) using the Python3 module PMOIRED[2], which allows the display and modelling of interferometric data stored in the OIFITS format. A telluric correction of the GRAVITY spectrum is performed to account for the fact that the interferometric quantities alone are only sensitive to the flux ratio. Notably, a strong Brγ line is visible across the observables. When fitting models with PMOIRED, the 'primary' is described as the central source, fixed at position (0,0) in the FoV. The flux of the primary star is normalised to 1 so it can be used as a reference point to determine the relative fluxes of any companions. Additionally, one can model any present emission lines in the fluxes and visible in the differential phases, by attributing Lorentzian or Gaussian line profiles to the model components. The fitting process was judged using the reduced chi-square statistic.

---

[1] https://www.mpe.mpg.de/~ott/QFitsView/

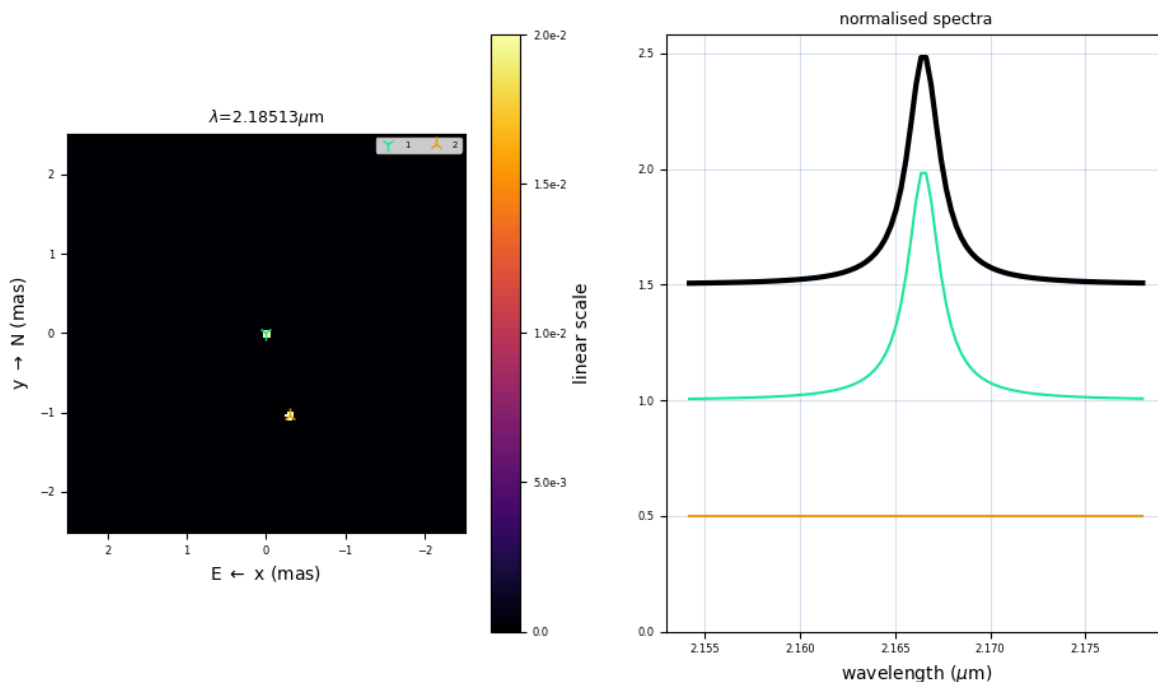[2] https://github.com/amerand/PMOIRED

Fig. 2. Model image (left) and synthetic spectra (right) corresponding to the best-fit model shown in Fig. 1. The green line corresponds to the primary star that is fixed at (0,0) and whose continuum flux is normalised to 1. The orange line corresponds to the secondary star. The black line is the total spectrum. The spectral line included in the model is at the Brγ wavelength.

3.2. Results

A variety of models were trialled including single star models, single disk models, binary disk models and triple systems. We refer the reader to Appendix B for an in-depth description of the fitting process. The best-fit to the GRAVITY data, with an example shown in Fig. 1, comes from a model composed of two sources, implying that a binary system with two optically bright companions is present at GRAVITY scales at a separation of ~1 mas across both epochs. Table B.1 displays the specific parameters resulting in the best-fitting model. We determine the errors on our derived measurements of the sources using bootstrapping. In the bootstrapping procedure, data is drawn randomly to create new datasets 200 times and the final parameters and uncertainties are estimated as the average and standard deviation of all the fits which were performed.

Figure 2 displays a model image and the synthetic spectra of the model components. Notably the dimmer star is on average 56% the flux of the brighter star and in this best fitting model the Brγ emission comes exclusively from the brightest star in the model.

3.3. An astrometric orbit

The interferometric data provide us with astrometric information on the luminous stars in the system. We feed this astrometric data into the SPectroscopic and INterferometric Orbital Solution finder (sPINOS, Fabry et al. 2021) to compare the movement of the system as constrained by interferometry to the orbit found by Bodensteiner et al. (2020a). Given the limited astrometric data, we opted to to fix the distance. Rivinius et al. (2020) suggested a distance of 310 ± 60 pc while Gaia yielded values of 342^{+25}_{-21} pc and 364^{+17}_{-16} pc in DR2 and eDR3, respectively (Bailer-Jones et al.

2018, 2021). It is, however, unclear how the presence of two optical components in HR 6819 impacts the Gaia distance estimate. **Astrometric excess noise can be caused by the high target brightness as well as by binarity and thus the purely statistical errors given by the 'parallax error' parameter of Gaia can be incomplete. For source 6649357561810851328 (HR 6819) the astrometric excess noise is marked as 0.857 mas for eDR3 at a significance level of 1180 and 0.731 mas at a significance level of 247 for DR2 and thus these two values overlap withing their error ranges.** Here we adopt a distance value of 340 pc, which sits comfortably within the estimated range of distances and is consistent with the distance value adopted in Bodensteiner et al. (2020a).

We further use the presence of the strong Brγ emission to identify the relative locations of the Be and B stars in the GRAVITY data, as the best interferometric fit determines that the emission is coming from the brighter star only. We also use the orbital parameters (P, i, T_0) of Bodensteiner et al. (2020a) as initial guesses as well as the measured RVs of the narrow-lined star to perform a first optimisation of the combined astrometric and RV data through the Levenberg-Markardt optimiser in sPINOS. The orbit was assumed to be circular. The obtained parameters then served as input for a full Markov-Chain Monte Carlo (MCMC) optimization where the period, inclination, time of perihelion passage, ascending node, semi-amplitude and total mass $(P, i, T_0, \Omega, K_1, \gamma_1,$ and M_{tot}, respectively) are varied simultaneously. The resulting best-fit astrometric orbit and RV curve are shown in Fig. 3.

The new astrometric data are simultaneously fit together with the RV measurements of the narrow-lined star with a fixed distance of 340 pc. We recover the orbital parameters of Bodensteiner et al. (2020a), except for a higher inclination of $49 \pm 2°$ (compared to their estimated value of ~32°) and
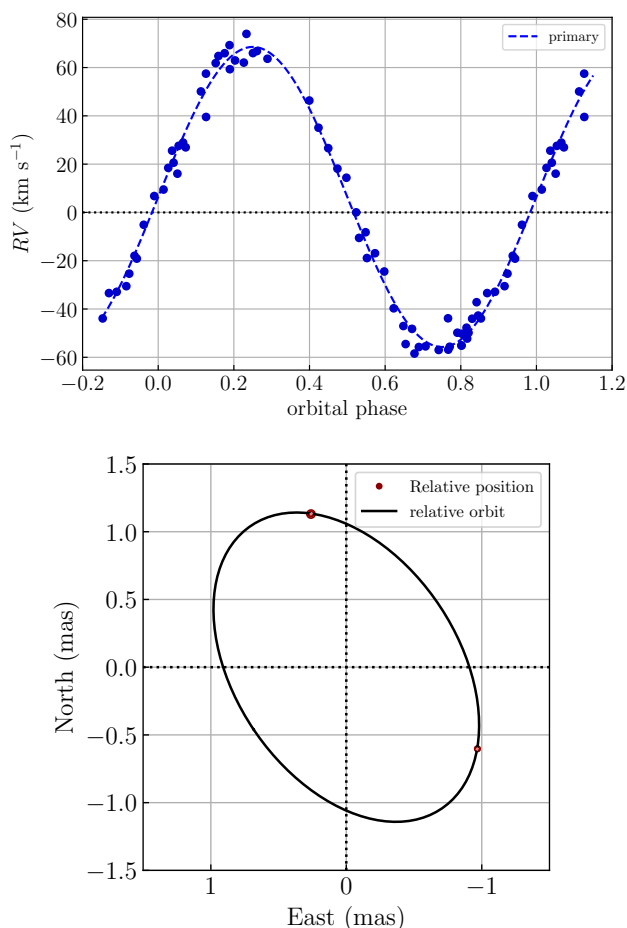
Fig. 3. Simultaneous fit to the stripped-B star FEROS RVs (upper panel) and the GRAVITY relative astrometry (lower panel), where the suspected stripped B-star is at coordinate (0,0). In doing so, we follow the definition of Bodensteiner et al. (2020a) for the identification of the primary and secondary components in the system. The MCMC grid can be found at the end of the appendix. **The adopted distance used for the plotted orbit on sky is 340 pc. The red dashed line in the top panel indicate the predicted amplitudes of the RV curve of the secondary star.**

a small adjustment of the ephemeris within the uncertainty of (Bodensteiner et al. 2020a) (Table C.1). Our combined solution yields a total mass for the system of $6.5 \pm 0.3 \, M_\odot$, with the errors estimated from the MCMC (Fig. C.1). This derived mass is in excellent agreement with the masses estimated from the atmospheric analysis of the Be and stripped B star scenario of Bodensteiner et al. (2020a). However, the estimated mass-ratio would yield $K_2 \approx 25 \, \mathrm{km \, s^{-1}}$, in stark contrast with the value of $4 \pm 1 \, \mathrm{km \, s^{-1}}$ estimated from spectral disentangling. An inclination of $35°$ would be needed to reconcile the two K_2 values. **A solution with the inclination fixed at $i = 37°$ is possible but the residuals of the astrometric solution increase from 11μas to 67μas. In this case, the derived total mass is $5.8 \pm 0.2 M_\odot$.**

Possible further avenues to reconcile both datasets include a much closer distance (~ 260 pc, Table C.1), larger statistical errors on the GRAVITY measurements, small systematic errors ($\sim 70 \mu$as) in the relative positions listed in Table B.1, or a combination of these.

The assumed distance indeed has a strong impact on the estimated total mass (Table C.1). Varying the distance by

+25 pc (or -30 pc) translates into a $\pm 1.5 \, M_\odot$ shift of the total mass. In addition, astrometric residuals of the fit of the order of 10μas clearly indicate that we are over-fitting the data, that is we are lacking a sufficient number of observational constraints with respect to the number of model parameters. Uncertainties are, in this situation, typically underestimated and the goodness-of-the-fit cannot be used as an estimate of the quality of the model. It is therefore clear that more GRAVITY data are a must if one is to obtain reliable estimates of the orientation of the orbit and of the individual masses of the components of HR 6819. More interferometric data would also help to lift the uncertainties surrounding the Gaia estimate.

Despite these limitations, the fact that the MUSE data described in the previous section detect no wide, bright companion, and the fact that GRAVITY shows two bright objects in a 40-day orbit lead us to conclude that the (B+BH)+Be triple system scenario should be excluded at a high confidence level.

4. Conclusions

In this letter we have presented new MUSE and GRAVITY data on the exotic source HR 6819 in order to distinguish between the two proposed hypotheses of the system's nature, the first of which suggests that HR 6819 is a triple system with an inner B star & BH binary and an outer Be star tertiary companion on a wide orbit (Rivinius et al. 2020) and the second suggesting that the system is a binary system consisting of a Be star and a B star that have previously interacted (Bodensteiner et al. 2020a; El-Badry & Quataert 2021). Should the former scenario be correct, a bright quasi-stationary companion should be present at ~100 mas. Should the latter scenario be correct, no bright companion should be detected at this separation and two bright stars should be detected at small separation.

Our MUSE data show no bright companion at ~100 mas separation. Our GRAVITY data resolve a close binary with ~1 mas separation composed of two bright stars. The GRAVITY spectra show the characteristic Brγ emission associated with a Be star decretion disk (Rivinius et al. 2013). Therefore, we conclude that HR 6819 is a binary system and reject the presence of a black hole on a short-period orbit in this system. HR 6819 therefore constitutes a perfect source to investigate the origin of Be stars and their possible formation through a binary channel. Looking to future work, further monitoring of the system with GRAVITY will be crucial. Not only can the orbit be better constrained, but these measurements will provide distance and precise mass estimates of what is likely a newly post-interaction, bloated stripped object and its associated Be star for the first time. Together with higher-resolution spectroscopy (e.g., from UVES), abundances of both stars could be derived. With this information, HR 6819 would constitute a corner-stone object to confront binary evolution models.

References

Abbott, B. P., Abbott, R., Abbott, T. D., et al. 2019, Physical Review X, 9, 031040
Abdul-Masih, M., Banyard, G., Bodensteiner, J., et al. 2020, Nature, 580, E11
Almeida, L. A., Sana, H., Taylor, W., et al. 2017, A&A, 598, A84
Bacon, R., Accardo, M., Adjali, L., et al. 2010, in Society of Photo-Optical Instrumentation Engineers (SPIE) Conference Series, Vol. 7735, Ground-based and Airborne Instrumentation for Astronomy III, ed. I. S. McLean, S. K. Ramsay, & H. Takami, 773508
Bailer-Jones, C. A. L., Rybizki, J., Fouesneau, M., Demleitner, M., & Andrae, R. 2021, AJ, 161, 147
Bailer-Jones, C. A. L., Rybizki, J., Fouesneau, M., Mantelet, G., & Andrae, R. 2018, AJ, 156, 58
Banyard, G., Sana, H., Mahy, L., et al. 2021, arXiv e-prints, arXiv:2108.07814
Bodensteiner, J., Shenar, T., Mahy, L., et al. 2020a, A&A, 641, A43
Bodensteiner, J., Shenar, T., & Sana, H. 2020b, A&A, 641, A42
de Mink, S. E., Langer, N., Izzard, R. G., Sana, H., & de Koter, A. 2013, ApJ, 764, 166
El-Badry, K. & Quataert, E. 2020, MNRAS, 493, L22
El-Badry, K. & Quataert, E. 2021, MNRAS, 502, 3436
Fabry, M., Hawcroft, C., Frost, A. J., et al. 2021, A&A, 651, A119
Gallenne, A., Mérand, A., Kervella, P., et al. 2015, A&A, 579, A68
Gies, D. R. & Wang, L. 2020, ApJ, 898, L44
Gravity Collaboration, Abuter, R., Accardo, M., et al. 2017, A&A, 602, A94
Hennicker, L., Kee, N. D., Shenar, T., et al. 2021, arXiv e-prints, arXiv:2111.15345
Irrgang, A., Geier, S., Kreuzer, S., Pelisoli, I., & Heber, U. 2020, A&A, 633, L5
Klement, R., Carciofi, A. C., Rivinius, T., et al. 2019, ApJ, 885, 147
Klement, R., Scott, N., Rivinius, T., Baade, D., & Hadrava, P. 2021, The Astronomer's Telegram, 14340, 1
Langer, N., Baade, D., Bodensteiner, J., et al. 2020, A&A, 633, A40
Lapeyrere, V., Kervella, P., Lacour, S., et al. 2014, in Society of Photo-Optical Instrumentation Engineers (SPIE) Conference Series, Vol. 9146, Proc. SPIE, 91462D
Lennon, D. J., Maíz Apellániz, J., Irrgang, A., et al. 2021, A&A, 649, A167
Liu, Q. Z., van Paradijs, J., & van den Heuvel, E. P. J. 2006, A&A, 455, 1165
Mahy, L., Almeida, L. A., Sana, H., et al. 2020a, A&A, 634, A119
Mahy, L., Sana, H., Abdul-Masih, M., et al. 2020b, A&A, 634, A118
Mason, B. D., Gies, D. R., Hartkopf, W. I., et al. 1998, AJ, 115, 821
Mazeh, T. & Faigler, S. 2020, MNRAS, 498, L58
Meilland, A., Millour, F., Kanaan, S., et al. 2012, A&A, 538, A110
Millour, F. 2014, in EAS Publications Series, Vol. 69-70, EAS Publications Series, 17–52
Moe, M. & Di Stefano, R. 2017, ApJS, 230, 15
Paczyński, B. 1971, ARA&A, 9, 183
Pols, O. R., Cote, J., Waters, L. B. F. M., & Heise, J. 1991, A&A, 241, 419
Rivinius, T., Baade, D., Hadrava, P., Heida, M., & Klement, R. 2020, A&A, 637, L3
Rivinius, T., Carciofi, A. C., & Martayan, C. 2013, A&A Rev., 21, 69
Rivinius, T., Štefl, S., & Baade, D. 2006, A&A, 459, 137
Safarzadeh, M., Toonen, S., & Loeb, A. 2020, ApJ, 897, L29
Sana, H., de Mink, S. E., de Koter, A., et al. 2012, Science, 337, 444
Shenar, T., Bodensteiner, J., Abdul-Masih, M., et al. 2020, A&A, 639, L6
Simón-Díaz, S., Maíz Apellániz, J., Lennon, D. J., et al. 2020, A&A, 634, L7
Sota, A., Maíz Apellániz, J., Morrell, N. I., et al. 2014, ApJS, 211, 10
Villaseñor, J. I., Taylor, W. D., Evans, C. J., et al. 2021, MNRAS, 507, 5348
Wang, L., Fujii, M. S., & Tanikawa, A. 2021, MNRAS, 504, 5778
Weigelt, G., Kraus, S., Driebe, T., et al. 2007, A&A, 464, 87
Weilbacher, P. M., Palsa, R., Streicher, O., et al. 2020, A&A, 641, A28

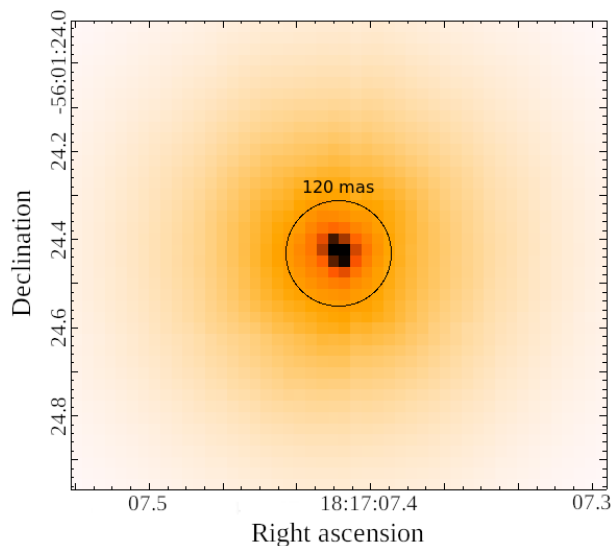**Fig. A.1.** Cut-out around the central source in the white-light image created by collapsing one of the unsaturated MUSE exposures.

Appendix A: Investigating the MUSE data

Figure A.1 shows a cut-out around the central source in one the MUSE exposures of HR 6819 which is created by collapsing the wavelength information in the MUSE data cube to obtain a white-light image.

Figure A.2 compares two extracted MUSE spectra with one epoch of FEROS observations (obtained at MJD = 53248.02 d). While one is extracted by summing up the central 5x5 pixel of the source (and therefore increasing the S/N), the second one is extracted just from the central pixel. The FEROS spectrum is downgraded to MUSE resolution and binning in wavelength. While slight differences are apparent, the overall spectra are quite similar and therefore indicate that the two stars making up the composite FEROS spectrum are within the central source visible in the MUSE data.

Appendix B: Modelling the GRAVITY data

Throughout the fitting process geometrical models were fit to the normalised K-band flux, the closure phases, the differential phases and the visibilities of the GRAVITY data using the code PMOIRED. The interferometric phases can tell us about asymmetries and the orientation of a system, whilst the visibilities describe the spatial extent of a source, with lower visibilities corresponding to a more resolved object (Millour 2014). A perfect cosine wave pattern should be generated in the $u - v$ plane for two point sources and the deviation of the observations from this is indicative of the position angle between the sources, the frequency of the cosine is related to the separation of the sources and the contrast of the wave pattern is indicative of the flux ratio.

Moreover, GRAVITY provides spectrally resolved data, and the pattern is wavelength dependent (with a known dependency), so that in the end the available measurements do very strongly over-constrain the system parameters (separation, PA, flux ratio). The GRAVITY data were taken in 2 polarisation planes, and the closure phase flips between these two datasets. Therefore, in order to reliably constrain the orientation of our system, the differential phase was of great importance. In our datasets a Brγ emission line is clearly visible in both the normalised flux
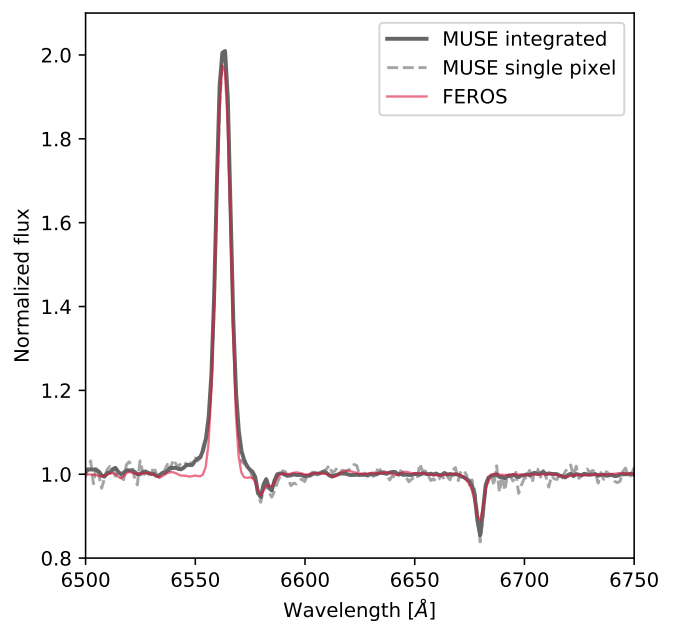

Fig. A.2. Comparison of two MUSE spectra of the central source, obtained by summing up the 5x5 central pixels (black) or extracting only the central pixel (gray), with a downgraded FEROS spectrum (red) at a similar phase.

and the differential phase. A double-peak is present in this line, particularly in the second epoch of the data (see Fig 1). Such a profile is often indicative of a rotating elongated structure such as a disk (e.g. Rivinius et al. 2013). Reproducing the Brγ line proved very useful during the fitting process in order to determine the nature of HR 6819, and we describe this process in this appendix.

A single star model provided a poor fit to the datasets, as did a triple. Using PMOIRED's detectionLimit method (the same as the approach implemented in the CANDID[3] software Gallenne et al. 2015) on our GRAVITY data, we find that a third companion within 100 mas of the binary must have a flux contrast of at most 2.0% (2.8%) in the K band compared to the primary, otherwise we would have detected it at the 3 σ (5 σ) level.

Binary models proved much more successful. One such model that presented a good fit was a binary model with an emission line associated with each star. The majority of the emission came from the brightest star in the system and was emitted at the central wavelength of Brγ with the remaining contribution to the line seen in the total flux coming from the dimmer star. The emission of the dimmer star in this model is slightly offset to shorter wavelengths, reproducing the double peak in the total flux. Brγ emission coming from both the stars in a Be post-interaction binary could be plausible, if some of the accreting material had failed to leave its Roche lobe and had created a small disk around the B star (as suggested in studies such as Shenar et al. 2020 and Hennicker et al. 2021). However, if this was the case, the emission of the two stars would be seen to switch throughout the orbit - the wavelength of the weaker emission line should change. This is not observed between the two epochs. Additionally, the superposition of two emission lines from each star could only reproduce the peak in the normalised flux, not the shape of the differential phase. Further modelling of disks around the B stars in stripped B+Be binaries and the generation of synthetic inter-
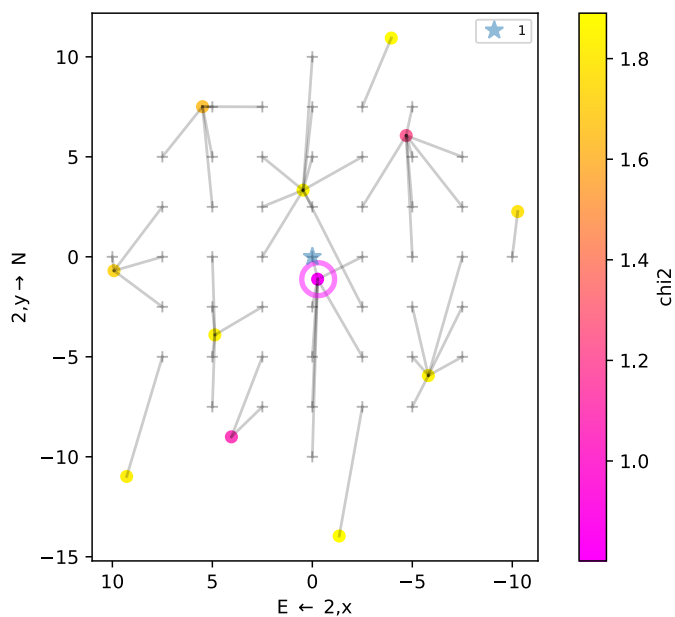
---

[3] https://github.com/amerand/CANDID

Fig. B.1. The grid-fit solution to the best-fitting model for a binary system with an emission line in one star. The figure shows the spatial positions that were mapped by the grid search as well as the associated reduced chi-square value of each of the tested positions (in color). The central star (whose position is not fit) is shown in blue, and the axes depict the space on the sky in arcseconds.

ferometric observables could help to better quantify the effects of this potential emission.

Since a model with two emission lines did not produce consistent results, we trialled a fit with two point sources where only one has an emission line. This resulting fit for such a model shows the Brγ emission coming from the brighter star in the binary, and provides an excellent fit to the data as quantified by the chi-square value. PMOIRED also possesses the capability to run a grid search to find the best model, based on the capabilities of an associated code, CANDID (Gallenne et al. 2015). Using this grid search on our datasets, the code determines that a two-point source model is the best option for the presented datasets, with an emission line in the brighter star. Figure B.1 shows the result of this grid search. However, such a model fails to reproduce the small double-peak feature (see Fig. 1). While the main peak seen in the differential phase is reproduced, the slight absorption feature is not. Despite the ambiguity, this implies that the brighter star in the system is most likely the Be star as Be star decretion disks are known to generate a surplus of Brγ emission and infrared excess (Rivinius et al. 2013).

The shape of the differential phase can provide key information on a system as it is a measure of the spatial offset of the line-emitting region with respect to the continuum emission (Millour 2014; Weigelt et al. 2007). For example, a 'V'-shaped differential phase can imply asymmetry or simple displacement of the photocentre, whilst an 'S'-shaped phase can imply rotation. Such 'S'-shapes are typical of disks, with Meilland et al. (2012) noting their presence in their spectro-interferometric VLTI/AMBER survey of Be stars. In our differential phases we observe a combination of these two features. Thus, we decided to determine whether a disk model could fit the observables. Uniform disk models were first attempted, but least-square fitting was unable to converge. Be stars are expected to have Keplerian rotating disks (Rivinius et al. 2006) so this was also trialled, but while more successful the code also struggled to converge to a physi-

cal solution. This could be due to the fact that the spatial extent of the disk is too small to be resolved by GRAVITY (<1 mas) whilst its emission persists in the total spectrum.

A toy model was used to see if the blue- and red-shifted emission could be used to help constrain the Keplerian fit. The model aimed to represent the emission of a Be star consisted of one point source with an associated emission line at the red-shifted wavelength, one point source with an emission line at the blue-shifted wavelength and one with no emission line meant to represent the centre of the disk. The dimmer star is modelled as a point source with no emission line. Figures B.2 and B.3 show the best-fit dataset and a visualisation of the model. The model provides a good fit to the data, particularly the second epoch, despite its nonphysical nature. The only caveat is that for the first dataset the visibilities are worse fit, but this is consistent as the separation of the blue and red shifted emission is not-technically resolvable with the VLTI.

We used this model to provide the starting parameters of another Keplerian disk fit. With these starting parameters, this Keplerian disk model could converge, resulting in the fits shown in Figures B.4 and B.5. The Keplerian model improves the shape of the model differential phase and normalised flux profiles further and is the only model to additionally fit the small peak feature in the visibilities as well. Again, the main caveat is that the size of the disk as determined through the fitting process is too small to be detected with the VLTI. With only two epochs the measure of the velocity structure of the disk is also likely unreliable.

Whilst the exact physical nature of the disk cannot be determined with our limited data-sets three things can be concluded from our GRAVITY data; 1) that the system is indeed a binary, as all the best-fitting models include two sources, 2) that the separation of these two sources is ~1 mas (across all models) and 3) the brighter star in the system is likely to be the Be star, given the convergence on a model with emission line in the brighter star and the successful (preliminary) detection of a disk around this brighter star. In the main body of text we present the simplest binary model (with Brγ emission in the brightest star) as our final model, given the uncertainty on the physical properties of this small disk obtainable with our dataset. Figures 1 and 2 shown in the main text correspond to this model. Table B.1 shows the details of the final model.

Appendix C: Orbital Details

Table B.1. Parameters derived from the GRAVITY fits of the final model. ρ is separation, PA is position angle. The position of the primary was fixed at (0,0). In this best-fitting model both stars are modelled as uniform disks with 0.2 mas diameters, such that they appear as point sources. f_K is the flux ratio of the dimmer star in the K-band in reference to the flux of the normalised brightest star (fixed to 1 during the fitting process). f_{line} is the flux of the Brγ line with respect to the continuum, w_{line} is **the full-width at half maximum (FWHM) of the line** and λ_{line} is its wavelength.

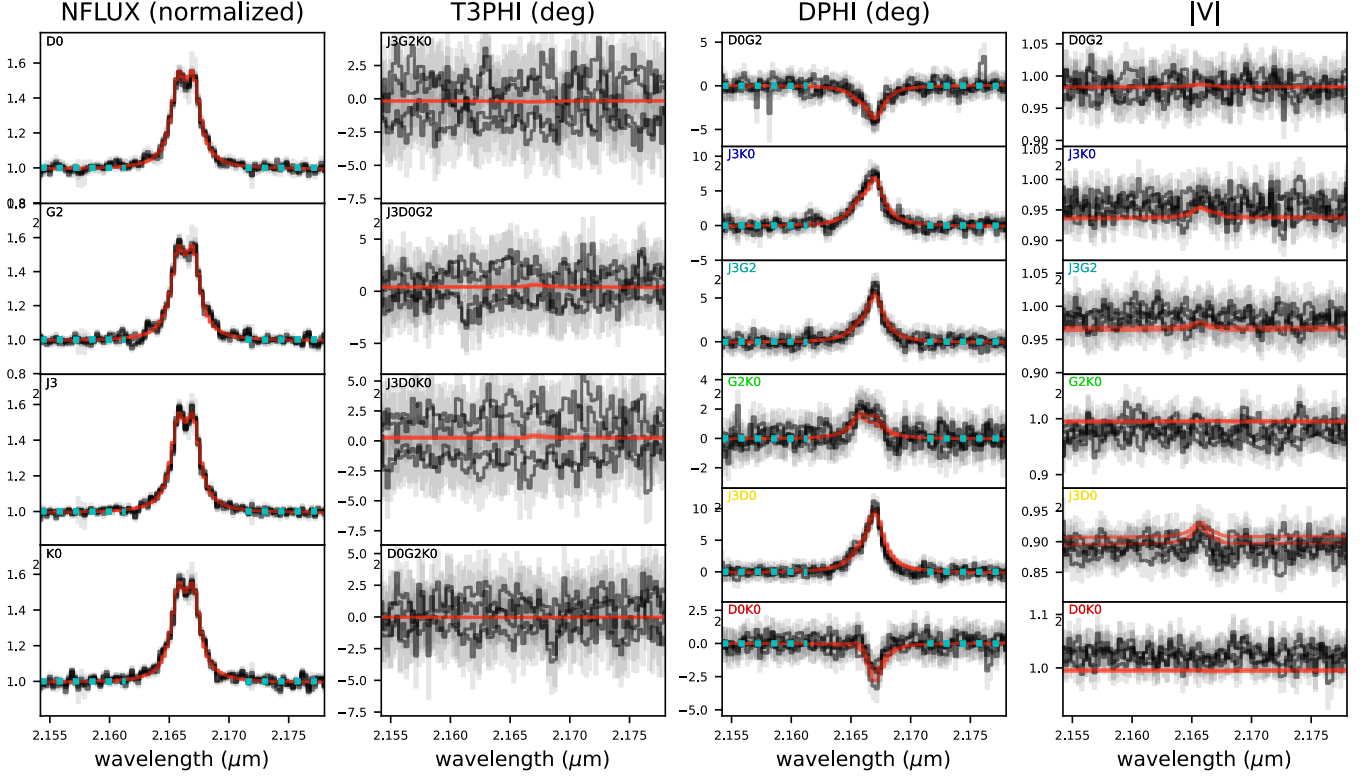| Mean Julian Date (MJD)	χ^2_{red}	f_K	ρ (mas)	PA ($^\circ$)	$f_{line,1}$	$w_{line,1}$ (nm)	$\lambda_{line,1}$ (μm)
59463.117	1.243	0.599±0.017	1.14±0.02	58.1±1	1.06±0.01	2.422±0.006	2.1661055±0.000002
59476.031	1.321	0.516±0.019	1.16±0.03	−167±0.8	0.892±0.001	2.643±0.004	2.166367±0.000001

Fig. B.2. Fits to the second GRAVITY dataset formed by a toy model composed of two point sources and two wavelength components surrounding the primary star (meant to mimic the blue- and red-shifted emission of a disk) that was run to obtain first guesses for the Keplerian fit. The inset labels are the baselines of the observations. NFLUX, T3PHI, DPHI and |V| refer to the normalised flux, closure phase, differential phase and visibilities respectively.
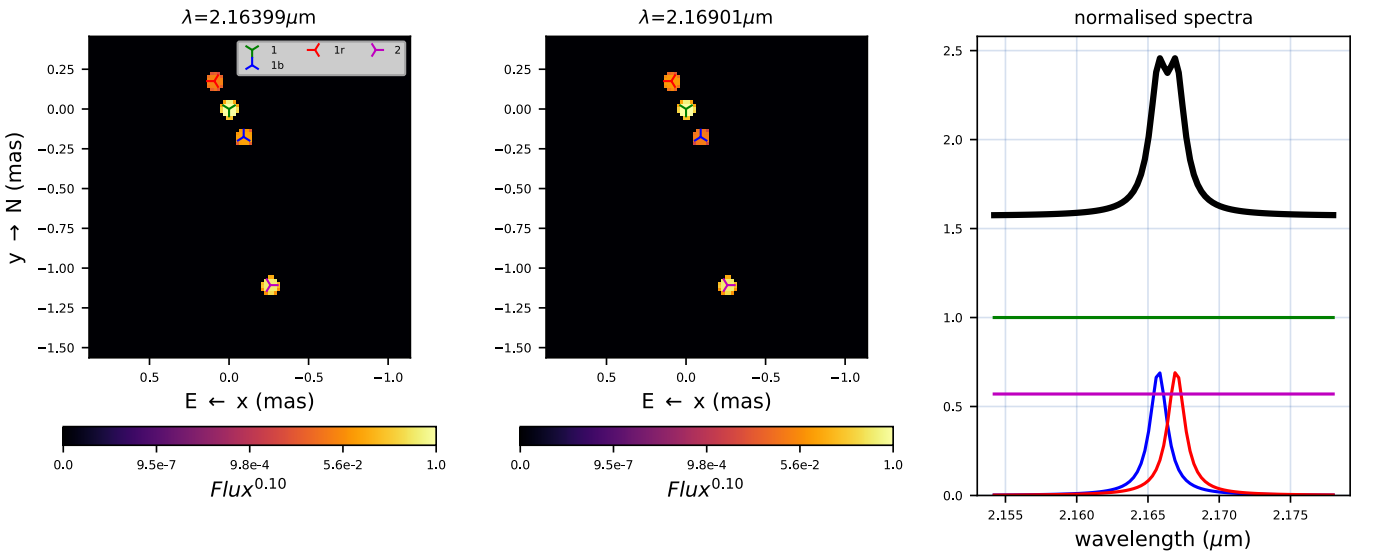

Fig. B.3. Model image and synthetic spectra for the toy model fit. The black line in the spectra is the total flux, the green is the brighter star's continuum flux, the purple is the dimmer star's continuum flux and the red and blue shifted emission is represented by the two remaining lines.
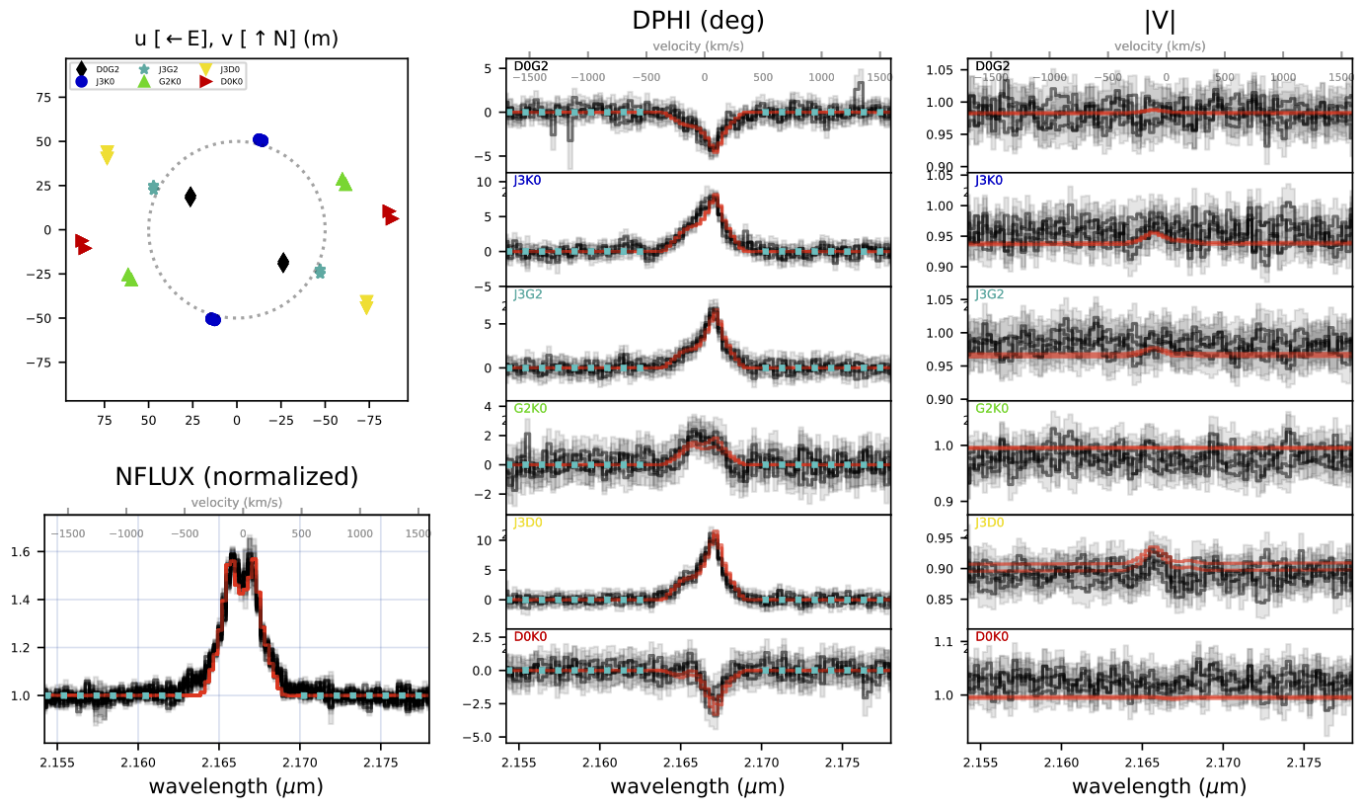
Fig. B.4. Fits to the second GRAVITY dataset from a model formed of Keplerian disk and two point sources. The inset labels are the VLTI baselines of the observations. NFLUX, T3PHI, DPHI and |V| refer to the normalised flux, closure phase, differential phase and visibilities respectively.
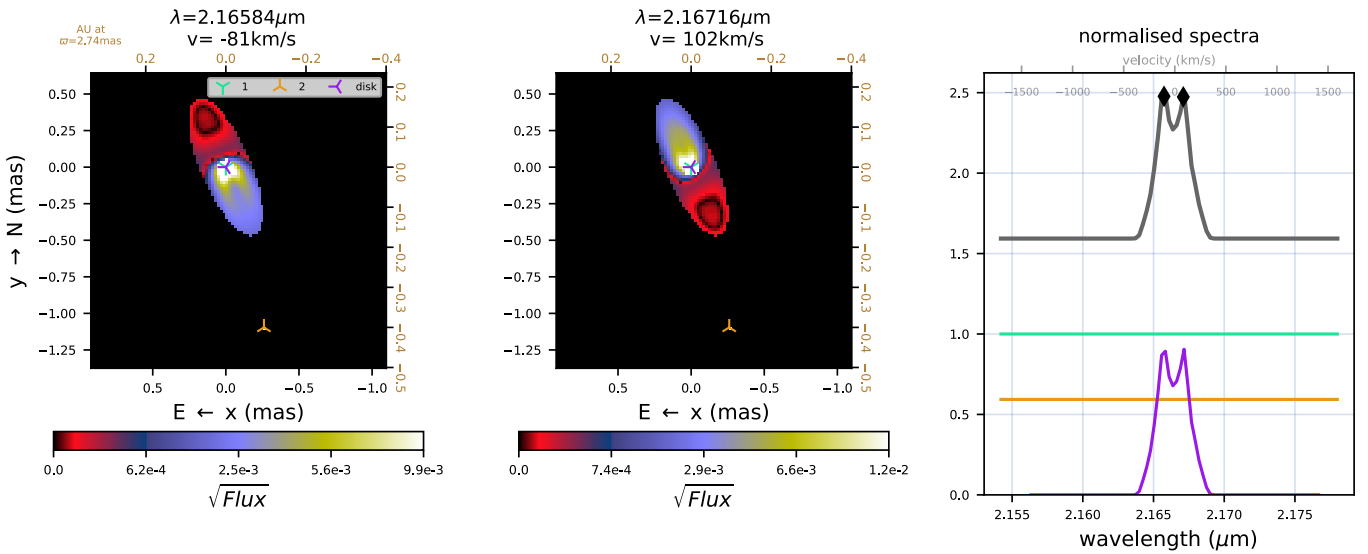

Fig. B.5. Model image and synthetic spectra for the toy model fit. The black line in the spectra is the total flux, the green is the brighter star's continuum flux, the orange is the dimmer star's flux, the purple is the disk's contribution to the flux.
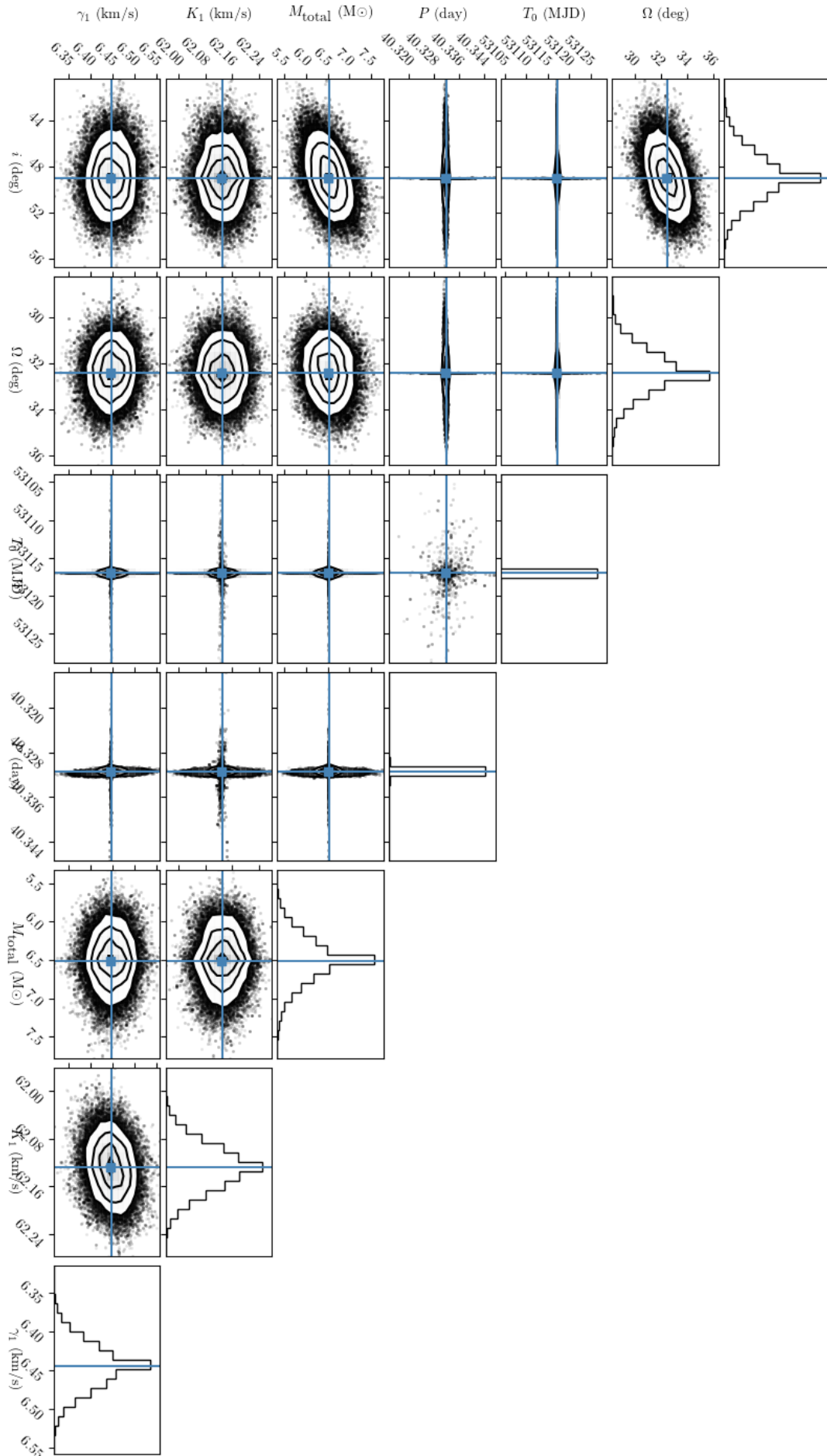
Fig. C.1. MCMC plot showing the error determination for the orbit shown in Fig. 3.

Table C.1. Parameters of the orbit derived determined by Bodensteiner et al. (2020a) compared to the current derivations for different assumed distances *D*. Circular orbits have been assumed in both works. MCMC were used the estimate the uncertainties.

Parameter	Bodensteiner et al. (2020a)		This work	
P_{orb} [d]	40.335 ± 0.007		40.3315 ± 0.0003	
T_0 [MJD] ($\Phi = 0$)	53116.9 ± 1.1		53116.918 ± 0.005	
γ [km s^{-1}]	9.13 ± 0.78		6.44 ± 0.03	
K_1 [km s^{-1}]	60.4 ± 1.0		62.13 ± 0.04	
Ω (°)	*n/a*		32.4 ± 0.9	
i [deg]	~ 32 (computed)		49.0 ± 1.9	
D (pc) [fixed]	340	340	364	258
M_{tot} [$M_\odot$]	~ 7.5 (computed)	6.5 ± 0.3	8.0 ± 0.4	2.8 ± 0.1
K_2 [km s^{-1}]	4.0 ± 0.8	~ 25 (computed)	~ 32 (computed)	~ 4 (computed)
rms$_{RV}$ (km s^{-1})			4.7	
rms$_{as}$ (μas)	*n/a*		11	